Oriented Cadmium Dihalide Particles Prepared in Langmuir–Blodgett Films

John K. Pike,[†] Houston Byrd,[†] Augusto A. Morrone,[‡] and Daniel R. Talham*,[†]

Department of Chemistry and Major Analytical Instrumentation Center, University of Florida, Gainesville, Florida 32611

Received March 25, 1994. Revised Manuscript Received June 13, 1994[⊗]

Oriented arrays of CdI_2, $CdBr_2$, and $CdCl_2$ particles have been synthesized in Langmuir–Blodgett (LB) films by the reaction of cadmium arachidate LB films with the corresponding hydrogen halide gas. Attenuated total reflectance FTIR (ATR-FTIR) shows that the conversions go to completion and that the organic film remains crystalline after reaction with the hydrogen halides. The cadmium halides are identified by transmission electron diffraction (TED) and X-ray photoelectron spectroscopy (XPS), and in each case only one inorganic species is formed. Transmission electron microscopy (TEM) and TED show that the CdI_2 particles are formed exclusively with their [001] crystal axes perpendicular to the plane of the LB film, and for domain sizes up to several square micrometers, discrete particles have the same in-plane orientation. The $CdBr_2$ and $CdCl_2$ particles are each observed to form with a mixture of two orientations, [001] axis parallel and [001] axis perpendicular to the LB plane. As with the iodide, domains are observed where arrays of particles exhibit common in-plane orientations. It is proposed that the organized organic matrix is responsible for orienting the inorganic particles, and potential lattice matching between the inorganic particles and the organic matrix is discussed.

Introduction

Organized organic assemblies have frequently been used in schemes to prepare inorganic particles where the organic structure serves as either a template or a reaction vessel of limited size. Examples of organic assemblies are micelles,[1] vesicles,[2,3] bilayer vesicles,[4] bilayer membranes,[5,6] polymeric matrices,[7] Langmuir monolayers,[8–18] and Langmuir–Blodgett (LB) films.[19] Inorganic materials that have been produced include semiconductors,[6,20,21] metallic particles,[22] and magnetic particles.[2,5,23] The goal is generally to produce inorganic particles with limited size[12,19,20,24] or limited dispersion,[16,25] and the approach draws inspiration from natural examples of organic-mediated crystallization of inorganic materials.[26]

An objective of our work is to develop methods for preparing single layers of inorganic extended lattice solids.[27–29] Such systems should allow for investigation of materials properties such as magnetism, conductivity, semiconductivity, or even superconductivity in the two-dimensional limit of a monolayer. Our approach uses layered organic assemblies, such as LB films or self-

[†] Department of Chemistry.
[‡] Major Analytical Instrumentation Center.
* Address correspondence to this author.
[⊗] Abstract published in *Advance ACS Abstracts,* July 15, 1994.

(1) Steigerwald, M. L.; Alivisatos, A. P.; Gibson, J. M.; Harris, T. D.; Kortan, A. R.; Muller, A. J.; Thayer, A. M.; Duncan, T. M.; Douglass, D. C.; Brus, L. E. *J. Am. Chem. Soc.* **1988**, *110*, 3046.
(2) Mann, S.; Hannington, J. P.; Williams, R. J. P. *Nature* **1986**, *324*, 565.
(3) Tricot, Y.-M.; Fendler, J. H. *J. Am. Chem. Soc.* **1984**, *106*, 7359.
(4) Mann, S.; Skarnulis, A. J.; Williams, R. J. P. *J. Chem. Soc., Chem. Commun.* **1979**, 1067.
(5) Zhao, X. K.; Herve, P. J.; Fendler, J. H. *J. Phys. Chem.* **1989**, *93*, 908.
(6) Baral, S.; Fendler, J. H. *J. Am. Chem. Soc.* **1989**, *111*, 1604.
(7) (a) Bianconi, P. A.; Lin, J.; Strzelecki, A. R. *Nature* **1991**, *349*, 315. (b) Lin, J.; Bianconi, P. A. *Polym. Prepr.* **1991**, *32*, 592.
(8) Rajam, S.; Heywood, B. R.; Walker, J. B. A.; Mann, S.; Davey, R. J.; Birchall, J. D. *J. Chem. Soc., Faraday Trans.* **1991**, *87*, 727.
(9) Heywood, B. R.; Rajam, S.; Mann, S. *J. Chem. Soc., Faraday Trans.* **1991**, *87*, 735.
(10) Landau, E. M.; Levanon, M.; Leiserowitz, L.; Lahav, M.; Sagiv, J. *Nature* **1985**, *318*, 353.
(11) Heywood, B. R.; Mann, S. *Langmuir* **1992**, *8*, 1492.
(12) (a) Zhao, X. K.; McCormick, L. D.; Fendler, J. H. *Langmuir* **1991**, *7*, 1255. (b) Zhao, X. K.; Yuan, Y.; Fendler, J. H. *J. Chem. Soc., Chem. Commun.* **1990**, 1248.
(13) Landau, E. M.; Popovitz-Biro, R.; Levanon, M.; Leiserowitz, L.; Lahav, M.; Sagiv, J. *Mol. Cryst. Liq. Cryst.* **1986**, *134*, 323.
(14) Landau, E. M.; Wolf, S. G.; Levanon, M.; Leiserowitz, L.; Lahav, M.; Sagiv, J. *J. Am. Chem. Soc.* **1989**, *111*, 1436.
(15) Heywood, B. R.; Mann, S. *J. Am. Chem. Soc.* **1992**, *114*, 4681.
(16) Zhao, X. K.; Yang, J.; McCormick, L. D.; Fendler, J. H. *J. Phys. Chem.* **1992**, *96*, 9933.
(17) Mann, S.; Heywood, B. R.; Rajam, S.; Birchall, J. D. *Nature* **1988**, *334*, 692.
(18) Mann, S.; Heywood, B. R.; Rajam, S.; Walker, J. B. A.; Davey, R. J.; Birchall, J. D. *Adv. Mater.* **1990**, *2*, 257.
(19) Smotkin, E. S.; Lee, C.; Bard, A. J.; Campion, A.; Fox, M. A.; Mallouk, T. E.; Webber, S. E.; White, J. M. *Chem. Phys. Lett.* **1988**, *152*, 265.
(20) (a) Xu, S.; Zhao, X. K.; Fendler, J. H. *Adv. Mater.* **1990**, *2*, 183. (b) Smotkin, E. S.; Brown, R. M.; Rabenberg, L. K.; Salomon, K.; Bard, A. J.; Campion, A.; Fox, M. A.; Mallouk, T. E.; Webber, S. E.; White, J. M. *J. Phys. Chem.* **1990**, *94*, 7543.
(21) (a) Zhao, X. K.; Fendler, J. H. *Chem. Mater.* **1991**, *3*, 168. (b) Geddes, N. J.; Urquhart, R. S.; Furlong, D. N.; Lawrence, C. R.; Tanaka, K.; Okahata, Y. *J. Phys. Chem.* **1993**, *97*, 13767. (c) Zhu, R.; Min, G.; Wei, Y.; Schmitt, H. J. *J. Phys. Chem.* **1992**, *96*, 8210. (d) Zhao, X. K.; Fendler, J. H. *J. Phys. Chem.* **1991**, *95*, 3716.
(22) (a) Kotov, N. A.; Zaniquelli, M. E. D.; Meldrum, F. C.; Fendler, J. H. *Langmuir* **1993**, *9*, 3710. (b) Sastry, M.; Mandale, A. B.; Badrinarayanan, S.; Ganguly, P. *Langmuir* **1992**, *8*, 2354.
(23) Zhao, X. K.; Xu, S.; Fendler, J. H. *J. Phys. Chem.* **1990**, *94*, 2573.
(24) (a) Scoberg, D. J.; Grieser, F.; Furlong, D. N. *J. Chem. Soc., Chem. Commun.* **1991**, *7*, 515. (b) Fendler, J. H. *Chem. Rev.* **1987**, *87*, 877. (c) Wang, Y.; Suna, A.; Mahler, W.; Kasowski, R. *J. Chem. Phys.* **1987**, *87*, 7315.
(25) Kimizuka, N.; Maeda, T.; Ichinose, I.; Kunitake, T. *Chem. Lett.* **1993**, 941.
(26) (a) Mann, S. *Nature* **1993**, *365*, 499. (b) Berman, A.; Addadi, L.; Weiner, S. *Nature* **1988**, *331*, 546. (c) Calvert, P.; Mann, S. *J. Mater. Sci.* **1988**, *23*, 3801. (d) Mann, S.; Frankel, R. B.; Blakemore, R. P. *Nature* **1984**, *310*, 405. (e) Mann, S. *Struct. Bonding (Berlin)* **1983**, *54*, 125. (f) Bromley, L. A.; Cottier, D.; Davey, R. J.; Dobbs, B.; Smith, S.; Heywood, B. R. *Langmuir* **1993**, *9*, 3594.

0897-4756/94/2806-1757$04.50/0

Scheme 1. Formation of Cadmium Dihalides within a Langmuir–Blodgett Template

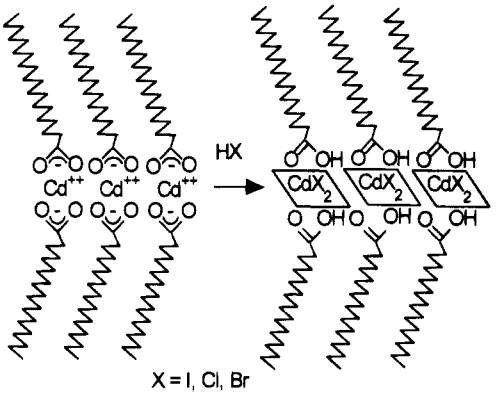

assembled monolayers, as templates for forming inorganic monolayers in analogy to how the organic assemblies described above have been used to form inorganic particles. For example, in a preparation that uses an LB film as a component of a mixed organic–inorganic layered solid,[30] we have reported monolayer and multilayer film analogues of the layered transition-metal phosphonates.[27,31] A different approach is to use the organic assembly to prearrange the metal ions into a layered array for further reaction that produces an extended inorganic lattice inside the organic matrix.[28,29] The idea is that the layered organic template should limit diffusion of the metal ions to individual planes of the organic matrix. If the inorganic solid has a layered structure, then the lattice energy may favor formation of single layers of the inorganic lattice. Our initial attempt (Scheme 1) at this approach targets the cadmium dihalides, CdX_2.[28] The "CdI_2" structure[32] is described by a hexagonal-close-packing of the anions in which every other layer of octahedral holes is occupied by a metal ion. The $CdCl_2$ and $CdBr_2$ structures are analogous to that of CdI_2 except for a cubic-close-packing of the chloride and bromide ions.[32] The structure of a single layer, however, is the same in both structure types. In these layered structures, the bonding within the anion–metal–anion layer is ionic–covalent, while the anion–anion interaction between layers is van der Waals in nature and easily cleaved.[32]

In a preliminary report, we described the reaction of cadmium arachidate LB films with gaseous HI to form CdI_2 particles within a layered arachidic acid matrix.[28] Although single CdI_2 layers have not yet been identified, electron diffraction studies showed that the template-formed CdI_2 is oriented exclusively with the CdI_2 layers parallel to the LB layers (CdI_2 [001] axis normal to the LB layer). In addition, for domain sizes up to several square micrometers, arrays of discrete particles are aligned with respect to one another about the [001] axis. The results suggest that the organic matrix is responsible for both orienting the CdI_2 particles and favoring crystal growth parallel to the LB planes. In this paper we present a complete report on the LB-formed CdI_2 along with characterization of $CdBr_2$ and $CdCl_2$ particles formed by the same method. The systems are characterized by attenuated total reflectance FTIR (ATR-FTIR), X-ray photoelectron spectroscopy (XPS), transmission electron microscopy (TEM), and transmission electron diffraction (TED). As with the formation of CdI_2 particles, $CdBr_2$ and $CdCl_2$ particles are produced with preferred orientations in the organic template, although two orientations of both the bromide and chloride are observed.

Experimental Section

Materials. Octadecyltrichlorosilane (OTS, $C_{18}H_{37}SiCl_3$, 95%) was obtained from Aldrich Chemical Co. (Milwaukee, WI) and stored under N_2 until use. Octadecanoic acid (stearic acid, $C_{17}H_{35}COOH$, 99.5%) was used as received from EM Science (Cherry Hill, NJ). Eicosanoic acid (arachidic acid, $C_{19}H_{39}COOH$, 99%) and cadmium chloride hemipentahydrate ($CdCl_2 \cdot 2^1/_2H_2O$, 98%) were purchased from Aldrich and used without further purification. Hydrogen bromide (99.8%), technical hydrogen chloride (99.0%), and hydrogen iodide (98.%) were obtained from Matheson Gas Products (Atlanta, GA). Spectrograde chloroform, hexadecane, and hexane were used as received. 300-mesh titanium electron microscope grids were purchased from the Ted Pella Company (Redding, CA). Formvar resin was purchased from Ted Pella and dissolved in spectrograde 1,2-dichloroethane before use. Silicon monoxide (325-mesh powder) was purchased from Aldrich. The water used as subphase in the LB experiment was purified via a Sybron/Barnstead Nanopure (Boston, MA) system immediately before use and had an average resistivity of 18 MΩ cm.

Substrate Preparation. For all XPS measurements, single-crystal (100) 20 × 15 × 1 mm^3 n- and p-type silicon wafers were purchased from Semiconductor Processing Co. (Boston, MA). For the infrared experiments, silicon ATR crystals, 45° 50 × 10 × 3 mm^3, were purchased from Wilmad Glass Company (Buena, NJ). The silicon XPS and IR substrates were cleaned using the RCA procedure[33] and dried under N_2. OTS was self-assembled[34] onto the silicon substrates by placing the clean substrates in a 2% solution of OTS in hexadecane for 30 min. Substrates were then rinsed in a chloroform Soxhlett extractor for 30 min. Upon removal from the Soxhlett, the substrates were hydrophobic. TEM substrates were electron microscope grids sandwiched between a 600 Å thickness of Formvar film and a 75 × 25 × 1 mm^3 glass microscope slide. A home-built electron-beam evaporator system was used to deposit 300 Å of SiO onto the Formvar layer at a rate of 1–2 nm/s as monitored by a quartz crystal microbalance. Pressure within the evaporator chamber was maintained at 4 × 10^{-8} atm. The basic TEM substrate preparation procedure is described in the literature.[35] The entire slide was then made hydrophobic with OTS as described above except that hexane was substituted for chloroform in the rinsing step.

Instrumentation. The LB films were deposited using a KSV Instruments (Stratford, CT) Model 5000 LB system with PTFE trough and hydrophobic barriers. The surface pressure was measured with a platinum Wilhelmy plate suspended from a KSV microbalance.

TEM and TED analyses were performed on a JEOL (Peabody, MA) JEM 200CX electron microscope. In all cases, the

(27) (a) Byrd, H.; Whipps, S.; Pike, J. K.; Ma, J.; Nagler, S. E.; Talham, D. R. *J. Am. Chem. Soc.* **1994**, *116*, 295. (b) Byrd, H.; Pike, J. K.; Talham, D. R. *Chem. Mater.* **1993**, *5*, 709. (c) Byrd, H.; Pike, J. K.; Showalter, M. L.; Whipps, S.; Talham, D. R. *ACS Symp. Ser., Chemically Sensitive Interfaces*, in press. (d) Byrd, H.; Pike, J. K.; Talham, D. R. *Thin Solid Films* **1994**, *242*, 100. (e) Byrd, H.; Whipps, S.; Pike, J. K.; Talham, D. R. *Thin Solid Films* **1994**, *244*, 768.

(28) Pike, J. K.; Byrd, H.; Morrone, A. A.; Talham, D. R. *J. Am. Chem. Soc.* **1993**, *115*, 8497.

(29) Pike, J. K.; Byrd, H.; Morrone, A. A.; Talham, D. R. *Thin Solid Films* **1994**, *243*, 510.

(30) Day, P. *Philos. Trans. R. Soc. London, Ser. A* **1985**, *314*, 145.

(31) Byrd, H.; Pike, J. K.; Talham, D. R. *J. Am. Chem. Soc.*, in press.

(32) Wells, A. F. *Structural Inorganic Chemistry*; Clarendon: Oxford, 1984.

(33) Kern, W. *J. Electrochem. Soc.* **1990**, *137*, 1887.

(34) (a) Netzer, L.; Sagiv, J. *J. Am. Chem. Soc.* **1983**, *105*, 674. (b) Maoz, R.; Sagiv, J. *J. Colloid. Interface Sci.* **1984**, *100*, 465.

(35) Fischer, A.; Sackmann, E. *J. Colloid. Interface Sci.* **1986**, *112*, 1.

electron beam was normal to the sample LB basal plane. Beam exposure was purposefully kept to a minimum to avoid sample degradation. Exposure times were typically less than 5 s for images and less than 11 s for diffraction patterns. The instrument was operated at 80, 100, and 200 kV as necessary, and the electron beam was collimated with a 200-μm-diameter condenser aperture. In some cases, focusing and other conditions were set in areas immediately adjacent to the region of interest, which was then shifted to the center of the image plane for photographic recording.

Infrared spectra were recorded with a Mattson Instruments (Madison, WI) Research Series-1 FTIR spectrometer using a narrow-band mercury cadmium telluride detector. A Harrick (Ossining, NY) TMP stage was used for the ATR experiments. All spectra consisted of 1000 scans at 2.0 cm^{-1} resolution and were referenced to the clean OTS-coated Si ATR crystal.

X-ray photoelectron spectra were obtained using a Perkin-Elmer (Eden Prairie, MN) PHI 5000 Series spectrometer. All spectra were taken using the Mg Kα line source at 1253.6 eV. The spectrometer has a typical resolution of 2.0 eV, with anode voltage and power settings of 15 kV and 300 W, respectively. Typical operating pressure was less than 5×10^{-9} atm. Survey scans were performed at a 70° takeoff angle with respect to the sample surface parallel using a pass energy of 89.45 eV. Multiplex scans, 20 scans over each peak, were run over a 45–50 eV range with a pass energy of 35.75 eV. Sample exposure to the X-ray beam and detector dead time were minimized to avoid unnecessary sample degradation.

Procedure. Langmuir–Blodgett films were prepared by spreading 100 μL of a 4.5 mM solution of stearic or arachidic acid in chloroform onto the subphase and allowing 15 min for the solvent to evaporate prior to compression. The subphase temperature was maintained at 16 ± 1 °C. For stearic acid and arachidic acid films, a pure water subphase was used (pH ≅ 5.2). Stearic acid and arachidic acid Langmuir monolayers were linearly compressed at a rate of 10 mN/(m min) to a surface pressure of 24 mN/m and deposited at rates of 25–50 mm/min. Transfer ratios were unity. Cadmium arachidate LB films were deposited from a 4 mM Cd^{2+} subphase pH-adjusted upward with KOH to pH 6.2 ± 0.1. The subphase was allowed to equilibrate for several hours prior to spreading over which time the pH was constant. The cadmium arachidate Langmuir monolayer was compressed linearly at a rate of 10 mN/(m min) to a surface pressure of 30 mN/m and deposited at rates of 25–50 mm/min with 10 min between successive dips for drying. Transfer ratios were unity.

Metal-halide-containing films were produced by exposing the LB films to the gaseous hydrohalic acids. The sample was placed within a glass test tube fitted with a sidearm stopcock valve and sealed with a rubber septum. The 80 mL tube containing the sample was evacuated and backfilled with dry Ar several times before 5 mL of gaseous HX was introduced through the rubber septum via gastight syringe. After a period of time the tube was purged with a positive pressure of dry Ar. Typical reaction conditions were 6.4×10^{-2} atm partial pressure of HX in argon for 5–15 min. Great care was taken throughout the procedure to avoid sample contamination.

Results

Attenuated Total Reflectance FTIR Spectroscopy. Reactions of the cadmium arachidate (CdArac) LB films with hydrogen halide (HX) gas were monitored by ATR-FTIR. Figure 1 shows the ATR-FTIR spectra from 1500 to 3500 cm^{-1} of 10-bilayer CdArac LB films before and after exposure to HCl, HBr, and HI. Peaks at 2953, 2917, and 2849 cm^{-1} in the CdArac spectrum (Figure 1, spectrum a) are the asymmetric methyl $\nu_a(CH_3)$, asymmetric methylene $\nu_a(CH_2)$, and symmetric methylene $\nu_s(CH_2)$ stretches, respectively, of the close-packed, all-trans hydrocarbon chains in the LB film.[36] The band at 1545 cm^{-1} is the asymmetric carboxylate stretch, $\nu_a(COO^-)$, characteristic of the metal carboxylate salt. The small peak at 1681 cm^{-1} is a carbonyl stretching band, $\nu(C{=}O)$ and appears as a result of incomplete salt formation in the LB film. At a pH of 6.2, used to deposit the CdArac films, we estimate 90–95% salt formation.[37] Upon exposure to HX (Figure 1, spectra b–d) the $\nu_a(COO^-)$ band completely disappears, and in all three cases a new band at 1701 cm^{-1} ($\nu(C{=}O)$) is observed, resulting from protonation of the amphiphile and formation of the carboxylic acid. There is no change in position, intensity, or fwhm of the methyl and methylene stretching bands, indicating that the organic layers do not undergo any gross changes in structure during the reaction, and that there is no loss of organic material under the reaction conditions used. In a series of control experiments, 10-bilayer films of metal-free arachidic acid were exposed to each of the hydrogen halides and no changes in the ATR-FTIR spectra were observed. In the arachidic acid and HX-exposed CdArac LB films, a broad absorbance between 3300 and 2500 cm^{-1} is observed which can be attributed to the acid O–H stretch. We do not observe any lattice or metal-coordinated water in the HX-exposed CdArac LB films.[38]

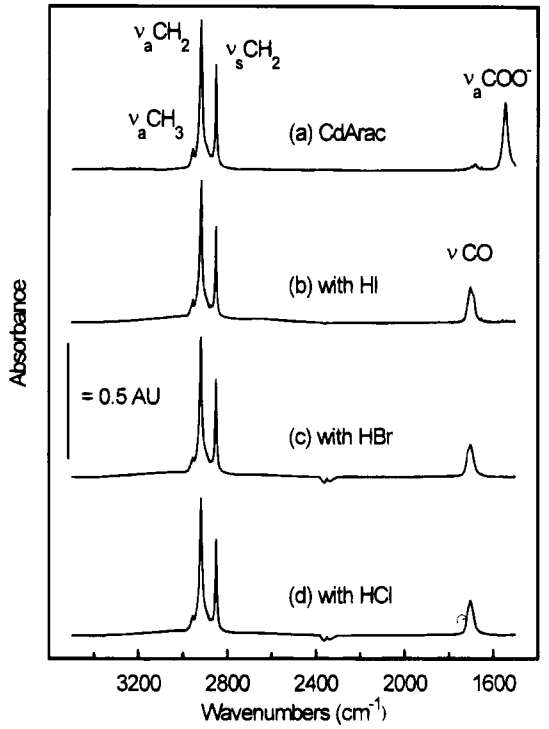

Figure 1. ATR-FTIR spectra of 10-bilayer LB films of cadmium arachidate: (a) before reaction and after 5-min exposure to (b) HI, (c) HBr, and (d) HCl. In spectra b–d, the disappearance of the $\nu_a COO^-$ band indicates that the reaction goes to completion.

X-ray Photoelectron Spectroscopy. Control experiments were run on stearic acid LB films to deter-

(36) (a) Wood, K. A.; Snyder, R. G.; Strauss, H. L. *J. Chem. Phys.* **1989**, *91*, 5255. (b) Porter, M. D.; Bright, T. B.; Allara, D. L.; Chidsey, C. E. D. *J. Am. Chem. Soc.* **1987**, *109*, 3559.

(37) (a) Ahn, D. J.; Franses, E. I. *J. Chem. Phys.* **1991**, *95*, 8486. (b) Peltonen, J.; Linden, M.; Fagerholm, H.; Györvary, E.; Eriksson, F. *Thin Solid Films* **1994**, *242*, 88. (c) Schwartz, D. K.; Viswanathan, R.; Garnaes, J.; Zasadzinski, J. A. *J. Am. Chem. Soc.* **1993**, *115*, 7374.

(38) Nakamoto, K. *Infrared Spectra of Inorganic and Coordination Compounds*; John Wiley & Sons: New York, 1963; p 155.

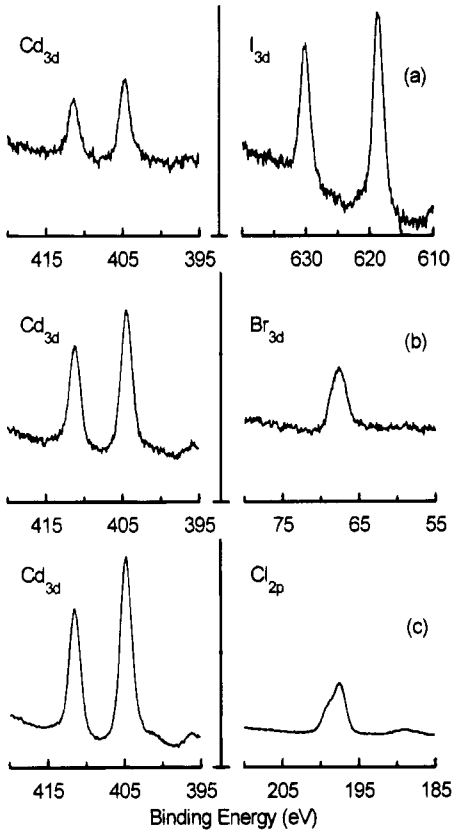

Figure 2. XPS spectra of 10-bilayer LB films of cadmium arachidate after 5-min exposure to (a) HI, (b) HCl, and (c) HBr. The observed relative M:X concentrations calculated in the text are (a) 32:68, (b) 45:55, and (c) 40:60.

mine whether the gaseous HX is incorporated into either the non-metal-containing LB film, the OTS layer, or the silicon substrate. Stearic acid LB films were exposed to each of the HX gases then placed in the XPS for study. XPS multiplex spectra over the appropriate halogen regions show that no halides are present in the non-metal-containing LB films.

Figure 2 presents XPS multiplex spectral data for 10-bilayer CdArac LB films after reaction with HCl, HBr, and HI. In each case, XPS reveals that the halogen is incorporated into the metal-containing film. The binding-energy peak areas are then integrated and corrected with an atomic sensitivity factor[39,40] to yield the observed relative concentrations for each element of interest (Table 1). The observed relative concentrations presented in Table 1 do not change over a wide range of HX-exposure conditions.

When using XPS to quantify elemental percentages in heterogeneous samples, the effects of photoelectron attenuation by an overlayer must be considered.[41] The inelastic mean free path, λ_m, of a photoelectron depends upon the photoelectron's kinetic energy and upon the material through which the escaping photoelectron travels. The XPS signal intensity, I, for any given element in the sample is reduced to the extent that that element's photoelectrons are attenuated by an overlayer.

Table 1. XPS Data

LB film/HX	peak	KE[d] (eV)	obsd rel concn, %	predicted rel concn,[e] %
CdArac/HI	Cd_{3d}	840	32 ± 3[a]	35
	I_{3d}	624	68	65
CdArac/HBr	Cd_{3d}	839	40 ± 2[b]	32
	Br_{3d}	1049	60	68
CdArac/HCl	Cd_{3d}	839	45 ± 4[c]	31
	Cl_{2p}	1179	55	69

[a] 95% confidence limits $N = 5$. [b] 95% confidence limits $N = 9$. [c] 95% confidence limits $N = 5$. [d] Kinetic energies are not corrected for peak-shifting due to sample charging effects. [e] Calculated for MX_2 stoichiometry from eq 2 in text using $\lambda_{Cd} = 319$ Å; $\lambda_I = 275$ Å; $\lambda_{Br} = 356$ Å; $\lambda_{Cl} = 378$ Å.

The relation is given by the attenuation equation[42] where I^∞ is the peak area normalization or sensitivity

$$I = (I^\infty)\exp(-d_m/(\lambda_m \sin\theta)) \quad (1)$$

factor,[40] d_m is the overlayer thickness of material m, λ_m is the inelastic mean free path of the photoelectron through material m, and θ is the takeoff angle with respect to the surface parallel. The relative concentration for element A, C_A, is then given by

$$C_A = \frac{\sum_A^\infty \exp(-d_{m,A}/\lambda_{m,A}\sin\theta)}{\sum_A^\infty \exp(-d_{m,A}/\lambda_{m,A}\sin\theta) + \sum_B^\infty \exp(-d_{m,B}/\lambda_{m,B}\sin\theta) + \ldots} \quad (2)$$

where the denominator is summed over all the elements of interest.[43] To model the cadmium halide–LB assembly, we assume a Y-type[44] matrix of tail-to-tail arachidic acid bilayers separated by CdX_2 monolayers where the topmost layer is an arachidic acid monolayer. For organic overlayers, values of λ_m are generally longer than those of inorganic overlayers[41] and estimates in the literature vary by about an order of magnitude.[41,45] For $\lambda_m \geq d_m$ however, the predicted relative concentrations for the Cd_{3d}, Cl_{2p}, Br_{3d}, and I_{3d} photoelectron peaks are nearly insensitive to changes in number of bilayers and changes in λ_m and vary by only about ±1% over the range of λ_m values in the literature.[41,45] Using the model described above and $d_m = 27.6$ Å for the thickness of a CdArac monolayer,[46] relative concentrations of 35.0% for Cd and 65.0% for I are predicted for a 1:2 Cd:I system in the LB matrix. This compares well with the observed relative concentration of 32% Cd to 68% I for

(39) *5000 Series ESCA Systems Version 2.0 Instruction Manual*; Perkin-Elmer Physical Electronics Division: Eden Prairie, MN, 1989.
(40) Wagner, C. D.; Davis, L. E.; Zeller, M. V.; Taylor, J. A.; Raymond, R. M.; Gale, L. H. *Surf. Interface Anal.* **1981**, *3*, 211.
(41) Seah, M. P.; Dench, W. A. *Surf. Interface Anal.* **1979**, *1*, 2.
(42) Seah, M. P. In: Briggs D., Seah, M. P., Eds.; *Practical Surface Analysis: Auger and X-Ray Photoelectron Spectroscopy*; John Wiley & Sons: Chichester, U.K., 1990; p 240.
(43) Holloway, P. H.; Bussing, T. D. *Surf. Interface Anal.* **1992**, *18*, 251.
(44) Roberts, G. *Langmuir–Blodgett Films*; Plenum Press: New York, 1990.
(45) (a) Akhter, S.; Lee, H.; Hong, H.-G.; Mallouk, T. E.; White, J. M. *J. Vac. Sci. Technol. A* **1989**, *7*, 1608. (b) Laibinis, P. E.; Bain, C. D.; Whitesides, G. M. *J. Phys. Chem.* **1991**, *95*, 7017. (c) Sastry, M.; Ganguly, P.; Badrinarayanan, S.; Mandale, A. B.; Sainkar, S. R.; Paranjape, D. V.; Patil, K. R.; Chaudhary, S. K. *J. Chem. Phys.* **1991**, *95*, 8631. (d) Ohnishi, T.; Ishitani, A.; Ishida, H.; Yamamoto, N.; Tsubomura, H. *J. Phys. Chem.* **1978**, *82*, 1989.
(46) (a) Brundle, C. R.; Hopster, H.; Swalen, J. D. *J. Chem. Phys.* **1979**, *70*, 5190. (b) Tippmann-Krayer, P.; Kenn, R. M.; Möhwald, H. *Thin Solid Films* **1992**, *210/211*, 577. (c) Jark, W.; Comelli, G.; Russell, T. P.; Stöhr, J. *Thin Solid Films* **1989**, *170*, 309.

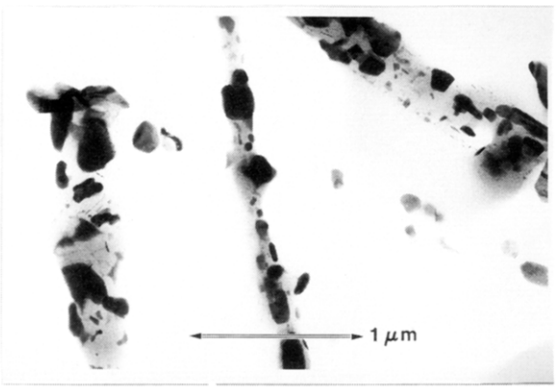

Figure 3. TEM image of a cast cadmium arachidate film after exposure to HI (30 000 magnification, 200 kV).

the HI-treated samples. For the CdArac–HBr system the observed relative concentrations, 40% Cd, and 60% Br, are exactly centered between the model's predictions for 1:2 and 1:1 Cd:Br stoichiometries. For the Cd:Cl systems, the observed relative concentrations are 45:55, while the model predicts relative concentration values of 32:68 and 49:51 for the 1:2 and 1:1 ratios, respectively. The XPS data are tabulated in Table 1 and are compared to the predicted relative concentrations calculated using the layered model with a CdX_2 stoichiometry.

Transmission Electron Microscopy. Control experiments were performed on LB films of arachidic acid to verify that the hydrogen halides do not react with either the un-ionized carboxylic acid, SiO, Formvar, or the Ti support grid. TEM images of multilayer arachidic acid LB films after HX exposure were featureless, and we have been able to record only diffuse scattering in electron diffraction measurements from the non-metal-containing LB films. Titanium support grids were used because copper grids react with the hydrogen halides. In another control experiment, a film of bulk CdArac was cast from hexane onto an electron microscope grid and then exposed to HI. Before reaction, the cast film appears as a random assortment of needles in the TEM, and only diffuse scattering is observed in diffraction. After exposure to HI, distinct particles are formed and appear in the micrograph as darker regions against the lighter organic material (Figure 3). The particles have an average size of about 0.1 μm. Electron diffraction from a 2.6-μm-diameter area of the HI-exposed cast film can be assigned to CdI_2, arising from a sample of randomly oriented particles.

CdArac LB films are featureless in the TEM, but yield crystalline diffraction in TED with the expected in-plane hexagonal symmetry and a d_{100} spacing of 4.26 ± 0.06 Å.[47] After exposing the CdArac LB film to HI, bright field TEM (Figure 4a) shows the appearance of particles. The observed particles range in size from 100 nm up to several micrometers across with an average size of about 0.4 μm. Some of the smaller particles have a hexagonal shape, while the larger crystallites lack well defined edges. TED from the HI-exposed CdArac LB film is shown in Figure 4b,c. During the diffraction experiment, Bragg spots from both the organic lattice and inorganic lattice are seen. The organic lattice diffraction pattern fades away within several seconds, while that of the inorganic lattice does not change position or orientation upon extended exposure to the electron beam.[28] TED from a larger, continuous particle (≥0.7 μm) is shown in Figure 4b and yields a single-crystal diffraction pattern corresponding to the CdI_2 [001] zone axis. Bragg spots corresponding to d spacings of 3.63 ± 0.06 Å, 2.12 ± 0.02 Å, and 1.38 ± 0.02 Å can be assigned to the {100}, {110}, and {120} reflections of CdI_2 and several orders of each reflection are seen.[48–50] Table 2 indexes the diffraction spots for the template-

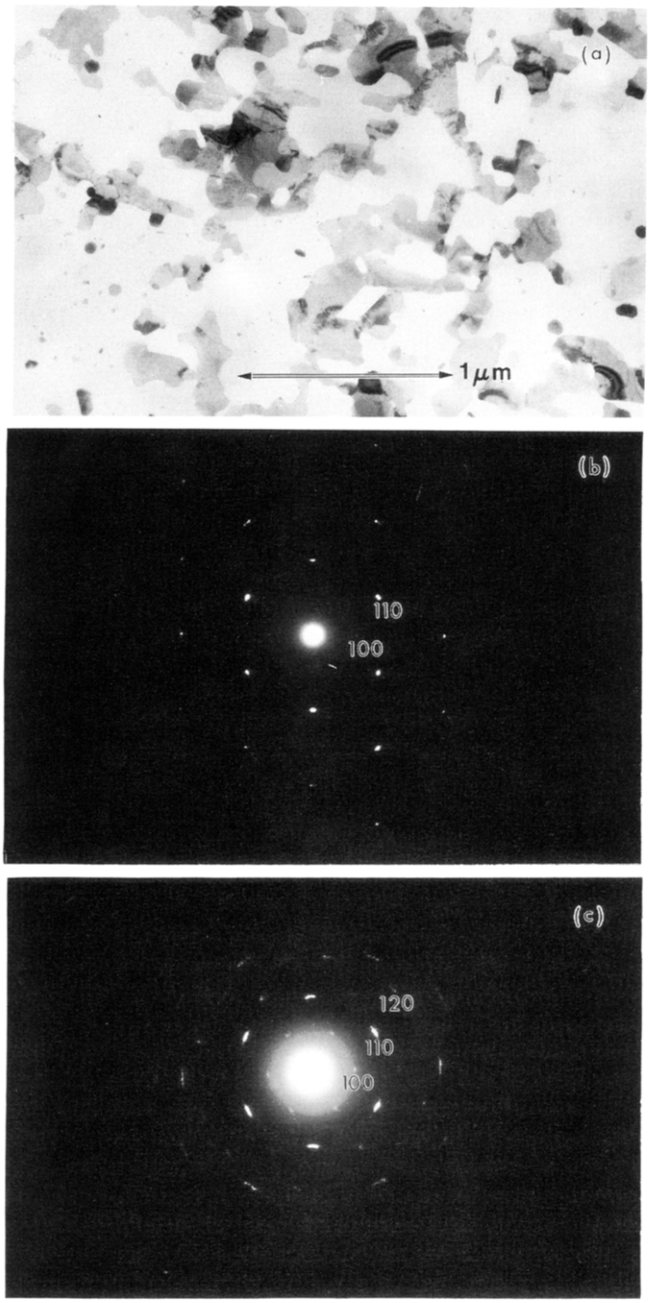

Figure 4. (a) TEM image of CdI_2 particles formed in a 10-bilayer cadmium arachidate LB film after reaction with HI (30 000 magnification, 200 kV). (b) 200 kV TED pattern from a single CdI_2 particle ≥0.7 μm in size. (c) 200 kV TED pattern from a 2.6-μm-diameter area in (a). The patterns in (b) and (c) correspond to the [001] zone axis of CdI_2. Diffracted spots can be assigned to the {100}, {110}, and {120} reflections of CdI_2.

(47) (a) Reigler, J. E. *J. Phys. Chem.* **1989**, *93*, 6475. (b) Inoue, T.; Yase, K.; Okada, M.; Okada, S.; Matsuda, H.; Nakanishi, H.; Kato, M. *Jpn. J. Appl. Phys.* **1989**, *28*, L2037. (c) Garoff, S.; Deckman, H. W.; Dunsmuir, J. H.; Alvarez, M. S.; Bloch, J. M. *J. Phys. (Paris)* **1986**, *47*, 701.

Table 2. Index of Transmission Electron Diffraction Data

	CdI_2		$CdBr_2$		$CdCl_2$	
hkl	*d*(obs) (Å)	*d*(lit.)[a] (Å)	*d*(obs) (Å)	*d*(lit.)[b] (Å)	*d*(obs) (Å)	*d*(lit.)[c] (Å)
100	3.63	3.69	3.4	3.42	3.31	3.33
110	2.12	2.12	1.99	1.98	1.93	1.93
120	1.38	1.38	1.29	1.29	1.26	1.26
200	1.8	1.83	1.67	1.71	1.66	1.67
220	1.05	1.06	0.99	0.99	0.96	0.96
130	1.01	1.02	0.94	0.95		
300	1.23	1.22	1.16	1.14	1.11	1.11
003			6.3	6.22	5.84	5.82
006			3.1	3.11	2.92	2.91
009					1.95	1.94
0012			1.59	1.56	1.46	1.45

[a] References 48 and 50 ($C\bar{3}m$). [b] Reference 61 ($R\bar{3}m$). [c] Reference 53 ($R\bar{3}m$).

formed particles by comparing them with the bulk CdI_2 *d* spacings.[48–50] The TED pattern in Figure 4c arises from a 2.6-μm-diameter area, and the dark field TEM of the same region shows that several discrete crystals contribute to this diffraction pattern. Like the single particle in Figure 4b, the observed diffraction from a group of several particles corresponds to the CdI_2 [001] zone axis. The diffraction spots have an angular variance of ±4° indicating that each particle has nearly the same in-plane orientation about the [001] zone axis.

To date we have been unable to reliably determine the thickness of the particles. Attempts to measure particle thickness have included sectioning the samples for viewing the cross section in TEM, measuring extinction contours[51,52] in the TEM, and low-angle X-ray diffraction. Estimates of particle thickness range from tens of angstroms to several hundred angstroms. These values may indeed represent the range of particle thicknesses present in the films. However, each of the methods used is complicated by the composite nature of the samples, and we feel that the spread in values is likely due to the uncertainty in the measurements.

Figure 5a–c presents typical TEM images and a TED pattern from particles resulting from the reaction of a 10-bilayer CdArac LB film and HBr. The particles can be grouped into two size categories: (1) large particles several hundred nanometers to one micrometer across; (2) small particles tens of nanometers in size. Figure 5a is an electron micrograph of several large particles which have been identified as $CdBr_2$ from electron diffraction (Table 2). Like the CdI_2 particles, diffraction from the large $CdBr_2$ particles gives rise to several orders of {*hk*0} reflections in a hexagonal pattern which originates from the [001] zone axis. At higher magnification, areas are observed where two types of smaller particles are grouped together in a relatively homogeneous distribution (Figure 5b). In these areas there are "needles", generally 10–50 nm long with an aspect ratio of about 10, and "round" particles 10–50 nm in diameter. Throughout the area shown in Figure 5b, the needlelike particles are oriented at about 120° relative to one another. The corresponding TED pattern is

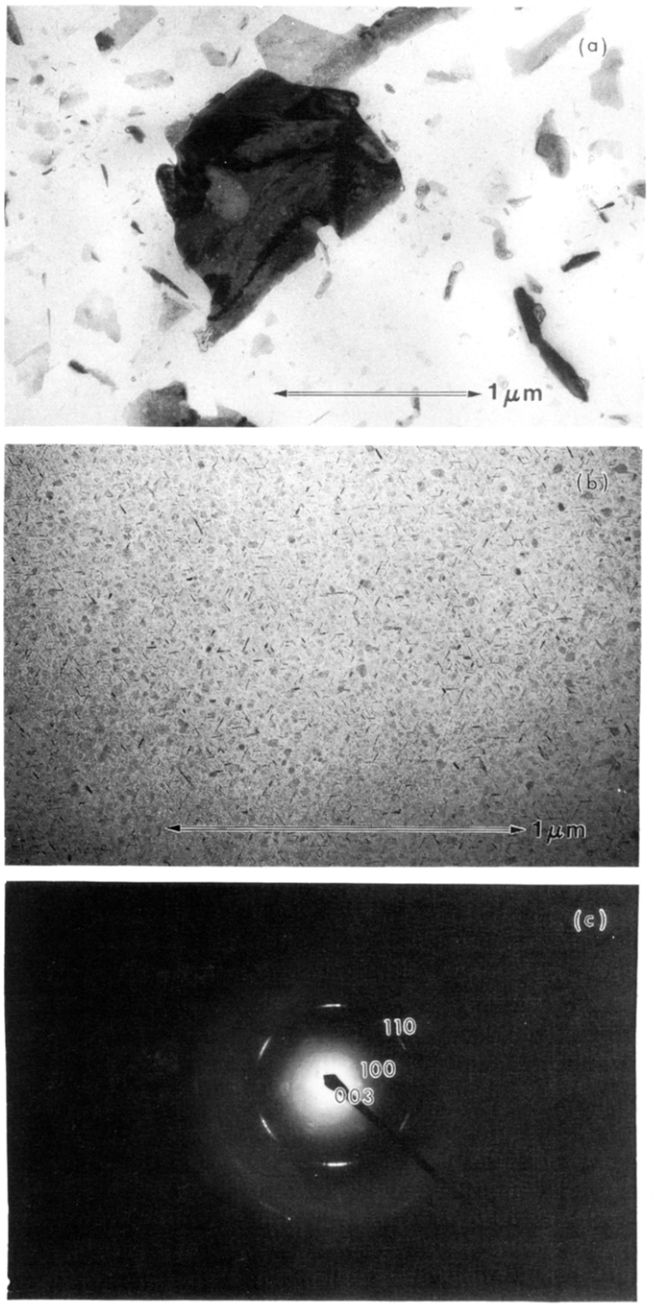

Figure 5. (a) TEM image of a typical "large" $CdBr_2$ particle formed in a 10-bilayer cadmium arachidate LB film after reaction with HBr (30 000 magnification, 200 kV). (b) TEM image of "smaller" $CdBr_2$ particles (50 000 magnification, 200 kV). Note the 120° relative rotation of the needles. (c) 200 kV TED pattern of a 0.7-μm-diameter area in (b). Diffracted spots can be assigned to either the {*hk*0} or {00*l*} reflections of $CdBr_2$.

shown in Figure 5c and presents evidence for two different orientations of the same crystallographic phase. Diffraction spots correspond to either {*hk*0} or {00*l*} $CdBr_2$ reflections, and several orders of each type of reflection are visible. The {*hk*0} reflections have an angular variance of ±10° and originate from crystals that have the [001] axis perpendicular to the LB plane. The limited angular variance indicates that the crystals giving rise to the {*hk*0} reflections are oriented relative to one another within the *ab* plane. The {00*l*} reflections are produced by the $CdBr_2$ particles that are oriented with the [001] zone axis parallel to the LB plane.

(48) Pinsker, Z. G. *Russ. J. Phys. Chem.* **1941**, *15*, 559.
(49) Wyckoff, R. W. G. *Crystal Structures*; Krieger: Florida, 1982.
(50) Finch, G. I.; Wilman, H. *Trans. Faraday Soc.* **1937**, *33*, 1435.
(51) Siems, R.; Delavignette, P.; Amelckx, S. *Phys. Status Solidi* **1962**, *2*, 421.
(52) Edington, J. W. *Practical Electron Microscopy in Materials Science*; Van Nostrand Reinhold: New York, 1976.

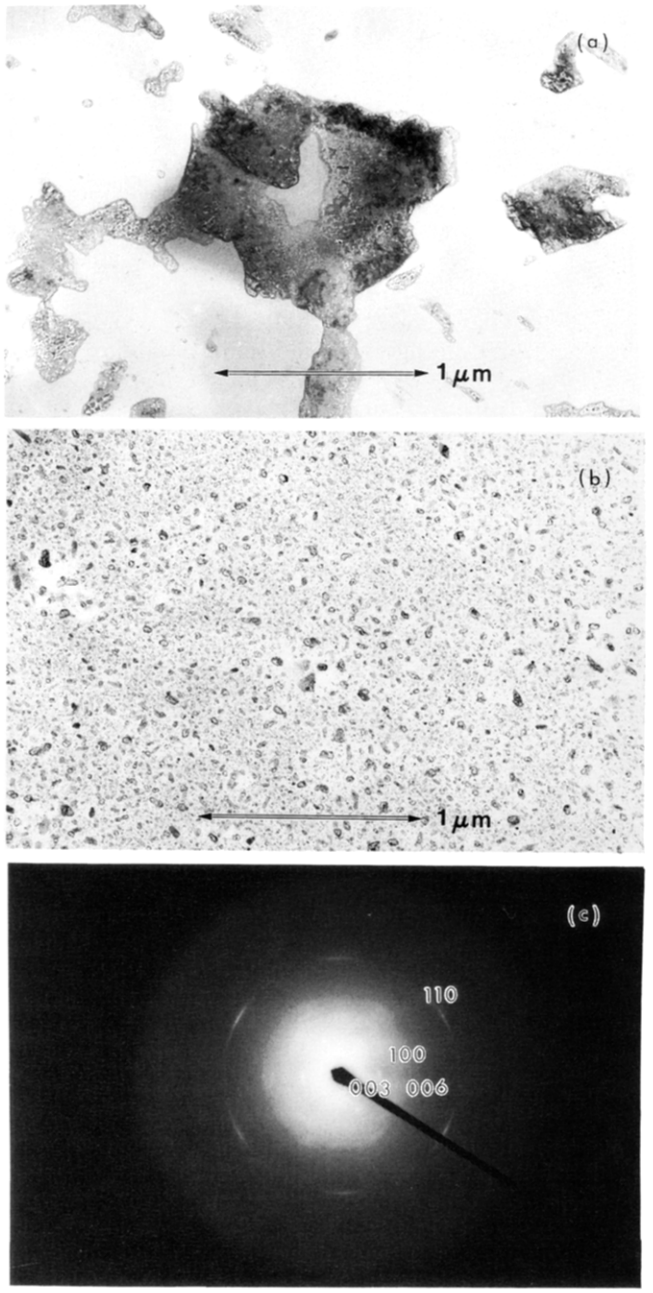

Figure 6. (a) TEM image a of typical "large" $CdCl_2$ particle formed in a 10-bilayer cadmium arachidate LB film after reaction with HCl (30 000 magnification, 100 kV). (b) TEM image of "smaller" $CdCl_2$ particles (30 000 magnification, 100 kV). (c) 100 kV TED pattern of a 2.6-μm-diameter area in (b). Diffracted spots can be assigned to either the $\{hk0\}$ or $\{00l\}$ reflections of $CdCl_2$.

TEM and TED results of HCl-exposed CdArac LB films are shown in Figure 6a–c. Large particles (Figure 6a) ranging from 100 to 600 nm in size are mixed with regions of homogeneously distributed smaller particles (Figure 6b) that range from 10 to 50 nm in size. Some of the larger particles are textured and appear to be aggregates of small particles. TED patterns can be indexed to the $CdCl_2$ structure, and, as for the $CdBr_2$ samples, two discrete sets of reflections are observed. Electron diffraction from some of the isolated larger particles gives rise to only $\{hk0\}$ reflections, while others give rise to a mixture of $\{hk0\}$ or $\{00l\}$ reflections. Electron diffraction patterns from large areas ($\geq$2.6-μm diameter) of evenly distributed smaller particles (Figure 6c) gives rise to strong {100} and {110} reflections as well as reflections from the $\{00l\}$ planes. The {110} Bragg spots have an angular rotation of $\pm 12°$. The complete indexing for the $CdCl_2$ TED data is listed in Table 2.[49,53]

Discussion

Organic Template Reaction. ATR-FTIR and XPS results confirm that the reaction of CdArac LB films with hydrogen halide gases goes to completion. The carboxylate is reprotonated in the reaction, and the halide is incorporated into the film forming the cadmium dihalide. The C–H stretching bands are unchanged after reaction suggesting that the organic lattice is intact with the hydrocarbon chains remaining crystalline and in an all-trans conformation. The reaction does not require high pressures of hydrogen halide and appears to be complete within a few seconds. All of the inorganic particles that are formed can be identified by electron diffraction as the corresponding cadmium dihalide, CdX_2. No other inorganic products are observed in the films by XPS and TED measurements. In addition, the XPS data coupled with the TED results indicate that all of the halogen in the films is in the form of the metal halide. When an un-ionized film of arachidic acid is reacted with HX, no halogen is observed in the film by XPS measurements. Halogens are seen only when the metal ion is present, and in each system, the cadmium-to-halogen ratio is independent of sample history (Table 1). For the CdI_2 system, the observed Cd:I ratio, determined by XPS, is exactly the ratio expected for the CdI_2 stoichiometry. In the $CdBr_2$ and $CdCl_2$ systems, the observed Cd:halogen ratios are greater than that predicted by the layered model (vide supra). A possible reason for the difference is oxide formation at the surface of the particles[54] which would increase the ratio of metal to halide observed in the XPS. Oxidation is more likely to occur at crystal edges, and as the average crystal size is reduced in the $CdBr_2$ and $CdCl_2$ samples, edge effects at crystal boundaries will have a greater effect on the observed relative elemental concentrations in these systems than in the CdI_2 samples. The LB films may also suffer damage due to photoelectrons generated in the XPS experiment.[55] We have observed higher rates of carbon loss for films containing the protonated fatty acid than for films containing the metal–carboxylate salt. Evidence for the desorption of whole molecules from protonated fatty acid LB films in the XPS has been reported by Kobayashi et al.[56] Loss of organic molecules in the LB film would tend to invalidate the layered model used to account for the effects of the photoelectron escape depth. Similarly, TEM images show that discrete particles of the cadmium dihalides are formed, indicating that the film geometry deviates further from the alternating layered matrix used to predict the relative elemental concentration. The most important observation from the XPS

(53) Pinsker, Z. G.; Tatarinova, I. *Russ. J. Phys. Chem.* **1941**, *15*, 1005.
(54) Peng, X.; Wei, Q.; Jiang, Y.; Chai, X.; Li, T.; Shen, J. *Thin Solid Films* **1992**, *210/211*, 401.
(55) Graham, R. L.; Bain, C. D.; Biebuyck, H. A.; Laibinis, P. E.; Whitesides, G. M. *J. Phys. Chem.* **1993**, *97*, 9456.
(56) Kobayashi, K.; Takaoka, K.; Ochiai, S. *Thin Solid Films* **1988**, *159*, 267.

data is that the cadmium-to-halogen ratios do not vary from experiment to experiment (Figure 2, Table 1) and are independent of reaction times and conditions. The fixed metal-to-halogen ratio for each system is consistent with the formation of only one inorganic species and with all of the halogen existing as the corresponding metal halide identified by TED.

Particle Orientation. It is well-known that CdArac LB films give rise to electron diffraction from domains of crystalline order up to several square micrometers in area.[47] In contrast to the solvent-cast films, exposure of CdArac LB films to HI, HBr, or HCl results in cadmium halide particles that exhibit preferential orientations relative to the substrate plane and relative to other particles. In the case of the CdI_2 system we find that, throughout the film, the particles are oriented *exclusively* with the [001] axis normal to the LB film basal plane. In other words, the metal halide layers are always parallel to the LB layers. By selecting an area of diffraction that includes many particles (Figure 4c), we observe single-crystal-like diffraction rather than polycrystalline-type rings. Not only do the particle basal planes share a common orientation, but domains exist as large as 2.6-μm in diameter, where the corresponding in-plane crystal axes have a common direction.

To account for the observed orientation in this experiment, we can consider two mechanisms. First, the CdArac precursor film organizes the cadmium ions into an arrangement similar to that found in the cadmium halides, and thereby directs the growth of the inorganic lattice by facilitating diffusion parallel to the LB basal plane and limiting diffusion between planes. Such a mechanism could account for the cadmium halide particles growing preferentially with the metal halide planes parallel to the LB plane. However, the observation of domains in which discrete cadmium halide particles have the same in-plane orientation suggests that some degree of lattice matching exists between the LB template and the cadmium halide and that this lattice match is responsible for directing the growth of particles.[57] This mechanism is analogous to how oriented particles are thought to grow at solution/monolayer interfaces.[8,10,11,13-18,58,59] In these studies, directionally mediated crystallization is thought to occur when there is geometric,[11,15,16] stereochemical,[10,14,17,19,58] or electrostatic[8,3,17] complementarity between the floating monolayer and the crystalline solid. At this point, we can only speculate about a potential lattice match between the CdI_2 particles and the LB film. Using a shorthand based on the Wood[60] notation, a $\sqrt{3}/2 \times \sqrt{3}/2)30°$ relation is found for the (001) surfaces of CdI_2 and the CdArac precursor, where $2a_{CdI_2} = \sqrt{3}a_{CdArac}$ (a is the unit cell of the parent lattice; $a_{CdI_2} = 4.24$ Å and $a_{CdArac} = 4.92$ Å).[47-49] The superposition of these two surface nets (Figure 7) is very nearly commensurate, having only a 0.5% lattice mismatch where the lattice mismatch is defined as $(\sqrt{3}a_{CdArac} - 2a_{CdI_2}/\sqrt{3}a_{CdArac}) \times 100$. Of course, after reaction with HI, the organic layer is no longer present as the cadmium salt and there may

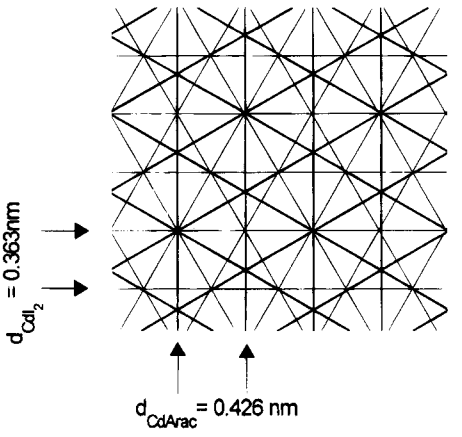

Figure 7. Line representation of the proposed $(\sqrt{3}/2 \times \sqrt{3}/2)30°$ relation for the (001) surfaces of CdI_2 and the cadmium arachidate LB film, drawn to scale. Bold lines represent the cadmium arachidate lattice; light lines show the CdI_2 lattice. The d spacings correspond to distances between (100) planes, and there is a 30° angle between the two lattice nets.

be some reorganization of the organic assembly to conform to the CdI_2 (001) surface. This reorganization would have to be cooperative and over a fairly long range to result in the observed orientation of discrete particles over a range of several micrometers.

In the $CdBr_2$-containing films a larger range of particle shapes and sizes is observed. The large $CdBr_2$ particles shown in Figure 5a give rise to many orders of $\{hk0\}$ reflections indicating that these particles are oriented with their [001] axis perpendicular to the LB plane. Electron diffraction from a collection of many discrete particles confirms that, within the LB plane, they are oriented with respect to each other as well. As in the CdI_2 case, there may be a lattice match between $CdBr_2$ and the organic lattice that accounts for the preferential orientation of the $CdBr_2$ particles. The same $(\sqrt{3}/2 \times \sqrt{3}/2)30°$ relationship suggested for the CdI_2 system results in a >7% mismatch in the case of $CdBr_2$. A potentially closer match is a $(^4/_5 \times ^4/_5)0°$ relationship between the (001) face of $CdBr_2$ and the basal plane of the precursor CdArac which would result in only a 0.4% mismatch, where $5a_{CdBr_2} \cong 4a_{CdArac}$ ($a_{CdBr_2} = 3.95$ Å and $a_{CdArac} = 4.92$ Å).[47,49,61] Electron diffraction from regions containing the smaller "needle-like" and "round" particles (Figure 5c) gives rise to two sets of reflections that can be indexed as the $\{hk0\}$ set and the $\{00l\}$ set of $CdBr_2$ reflections. In a single-crystal pattern, these reflections cannot be produced simultaneously because their respective zone axes are normal to one another.[52] The observed diffraction pattern then, is produced from two sets of $CdBr_2$ crystals with distinct orientations. One set is oriented with the [001] direction perpendicular to the LB plane, producing the $\{hk0\}$ reflections, while the other set of crystals is oriented with the [001] direction parallel to the LB plane, producing the $\{00l\}$ reflections. Attempts to isolate each set of crystals using dark field imaging were unsuccessful due to the low intensity of the scattered beams. Figure 5c shows that the $\{00l\}$ reflections are aligned with the $<h00>$ directions and also produce a hexagonal pattern. Since the sets of planes that give rise to the

(57) van der Merwe, J. H. *Philos. Mag. A* **1982**, *45*, 127.
(58) Weissbuch, I.; Addadi, L.; Leiserowitz, L.; Lahav, M. *J. Am. Chem. Soc.* **1988**, *110*, 561.
(59) Popovitz-Biro, R.; Lahav, M.; Leiserowitz, L. *J. Am. Chem. Soc.* **1991**, *113*, 8943.
(60) Wood, E. A. *J. Appl. Phys.* **1964**, *35*, 1306.
(61) Pinsker, Z. G. *Russ. J. Phys. Chem.* **1942**, *16*, 1.

{00*l*} reflections have only 2-fold symmetry, a hexagonal pattern can only be produced if there are multiple orientations of the crystals related by 3-fold symmetry. In Figure 5b, the needlelike particles are clearly pictured with three preferred orientations rotated by 120° with respect to one another. This 3-fold orientation of the needlelike particles may be a consequence of the in-plane hexagonal-close-packing of the alkyl chains in the LB film. If indeed the needlelike particles give rise to the {00*l*} reflections, then the small "round" particles must give rise to the {*hk*0} reflections and are oriented, like the large $CdBr_2$ particles, with their [001] axis perpendicular to the LB basal plane. The round particles are also oriented with respect to one another within the LB plane, although the angular variance is greater than that observed in the CdI_2 system.

$CdCl_2$, like $CdBr_2$, is also formed in oriented arrays. The $CdCl_2$ particles grow with their [001] axis either parallel or perpendicular to the LB plane. Unlike the $CdBr_2$, the observation of the two types of $CdCl_2$ particles is not as dramatic in the electron micrograph. For each set of crystal diffraction, however, the absence of polycrystalline rings requires that large groups of discrete particles share a common orientation within the LB plane. Also, like the $CdBr_2$, the $CdCl_2$ {00*l*} reflections have 3-fold symmetry in the diffraction pattern indicating that the crystals giving rise to these reflections must have three orientations.

Lattice Matching. Comparing the three systems, we observe larger, more contiguous CdI_2 particles than either of the other metal halides. In some cases, single CdI_2 particles up to 5 μm across are observed. When selecting arrays of several particles, electron diffraction from the CdI_2 sample is sharper and more single-crystal-like than from similar arrays of $CdBr_2$ and $CdCl_2$. The CdI_2 particles sampled in Figure 4 are oriented by ±4° about the [001] zone axis while those particles giving rise to the same reflections in the $CdBr_2$ and $CdCl_2$ systems, although still oriented, show a wider variance of in-plane alignment, up to ±12° in the $CdCl_2$ sample. If lattice matching with the organic template is responsible for the observed particle orientation, this suggests that the lattice match is closer for CdI_2 than for either $CdBr_2$ or $CdCl_2$. Comparing the $(\sqrt{3}/2 \times \sqrt{3}/2)30°$ relationship between the (001) faces of the metal halide and the hexagonal close packing seen in CdArac, it is clear that the match is closest for CdI_2. Of course, the potential lattice match does not need to be the same in all three cases. With all three systems, however, the organic template is expected to conform somewhat to the inorganic extended lattice.[57] There is a limit to the extent the LB film can deform before strain develops, resulting in defects and domain boundaries. If the LB layer does play a role in mediating particle growth, such strains could limit particle size as well as the extent of particle alignment and may account for the smaller particles and lower degree of orientational order observed for the bromide and chloride samples. Defect sites in the LB film could also be effective nucleation sites for crystals to grow with alternative orientations such as those observed in the $CdBr_2$ and $CdCl_2$ systems.

Conclusion

The observation that CdI_2, $CdBr_2$, and $CdCl_2$ are formed with specific orientations within an LB film provides a further example that an organized organic template can be used to direct the growth of inorganic particles. The complementarity between the layered structure of the cadmium dihalide and the layered organic template may play a role in orienting the particles. While a single layer of an inorganic lattice has not yet been identified using this type of organic template-directed synthesis, the observation of oriented arrays of inorganic particles is encouraging. The results suggest that with the proper choice of inorganic lattice and organic template, single layers may be isolable.

Acknowledgment. We thank Mr. Eric Lambers, Dr. Vladimir I. Levit, and Vera Romanskayya for technical assistance. Acknowledgement is made to the National Science Foundation [DMR-9205333] and the University of Florida Division of Sponsored Research for partial support of this research.